Impact of aluminum fluoride addition on crystallization, structure and thermal properties of lead borate glasses

Yu. S. Hordieiev[*], A. V. Zaichuk
Ukrainian State University of Chemical Technology, 8 Gagarin Avenue, Dnipro, 49005, Ukraine

The glass composition $(70-x)$PbO–$(30-y)$B$_2$O$_3$–$(x+y)$AlF$_3$, where x and y ranges from 0 to 20 mol%, were prepared using the conventional melt-quenching-annealing technique. The structural and thermal properties of the glasses were comprehensively analyzed using techniques like Differential Thermal Analysis (DTA), Dilatometry, Fourier-Transform Infrared Spectroscopy (FTIR), X-ray Diffraction (XRD), and Scanning Electron Microscopy (SEM). XRD confirmed the amorphous, non-crystalline structure of the glasses. The glass network was found to be composed of structural units such as PbO$_4$, BO$_4$, BO$_3$ and AlO$_6$ using FTIR spectroscopy. FTIR analysis revealed significant structural changes, including the transformation of BO$_4$ to BO$_3$ units and the increase in non-bridging bonds, particularly with higher AlF$_3$ content. DTA was instrumental in determining characteristic temperatures, such as the glass transition, melting, and peak crystallization temperatures, along with glass stability parameters (ΔT, Hr, T$_{gr}$) for all samples. The study found that the addition of AlF$_3$ led to a decrease in these characteristic temperatures when replacing B$_2$O$_3$, but an increase when replacing PbO. Variations in the density and thermal expansion of the lead borate glass were observed upon the addition of AlF$_3$, decreasing when substituting for PbO and increasing when substituting for B$_2$O$_3$. These findings provide insights into the properties of oxyfluoride glasses, paving the way for future optimization in their composition for varied applications.

1. Introduction

Lead borate glasses occupy an important position in materials science, particularly in the field of optical and electronic applications. Known for their low-temperature melting, high refractive index and optical nonlinearity, lead borate glasses are gaining increasing importance due to their potential in optoelectronics, acousto-optics and other advanced applications [1–3]. Incorporating heavy metal oxides such as PbO into borate glasses has been shown to lower the melting point and improve chemical resistance, making these glasses suitable for producing robust and reliable seals [4, 5]. These seals are particularly useful in encapsulating electronic components, ensuring their longevity and functionality. Moreover, glasses with high PbO content are also used for radiation shielding in medical and nuclear applications [6, 7].

In recent years, the focus has shifted towards oxyfluoride glasses, which combine the beneficial properties of oxide and fluoride glasses. The merging of oxide and fluoride components in oxyfluoride glasses creates a balance, harnessing the mechanical and thermal stability of oxides and the low phonon energy of fluorides [8]. This combination is ideal for hosting rare earth ions in optical materials, offering significant potential in fields like optoelectronics and photonics [9]. Particularly, the addition of AlF$_3$, CdF$_2$ and PbF$_2$ to heavy metal oxide borate glasses is a fascinating field of study as these additives have a significant effect on the structure, crystallization, thermal and optical properties of the glasses [10–13]. Incorporating these additives can reduce the phonon energy and increase the overall transparency of the oxyfluoride glasses,

---

[*] Corresponding author: yuriihordieiev@gmail.com

both of which are critical for optical applications [14]. Additionally, the substitution of oxygen for fluorine within the lead borate glass structure results in reduced viscosity and melting points, as well as increased electrical conductivity and activation energy [15, 16]. Investigating the impact of these additives on lead-borate glass is not only scientifically exciting but also critical to advancing the performance and versatility of these materials in a range of high-tech applications. This line of research could pave the way for creating more efficient, resilient, and adaptable glass-based materials, with broad-reaching implications in sectors such as telecommunications, laser technology, and photonics.

The current study aims to investigate the impact of AlF_3 addition on the structure, crystallization behavior and thermal properties of $70PbO–30B_2O_3$ glass. The research utilizes X-ray diffraction (XRD), scanning electron microscopy (SEM), Fourier-transform infrared spectroscopy (FTIR), differential thermal analysis (DTA), and dilatometry techniques to comprehensively investigate the topic.

2. Materials and methods

Table 1 provides a comprehensive list of oxyfluoride lead aluminoborate glass compositions, with each composition labeled for easy reference. These glasses were prepared with a molar composition of $(70-x)PbO–(30-y)B_2O_3–(x+y)AlF_3$, where x and y range from 0 to 20 mol%. The production process involved the utilization of raw materials, namely Pb_3O_4 (99.5%, Colorobbia), H_3BO_3 (99.9%, Eti Mine Works), and AlF_3 (99%, Reachim). These components were meticulously mixed using an agate mortar and subsequently melted in a 50 mL platinum crucible, employing an electric furnace equipped with silicon carbide (SiC) heaters, at a temperature of 850°C for a duration of 45 minutes. Following the melting process, the molten glass was promptly poured into a preheated stainless steel mold. Subsequently, the glass samples underwent an annealing procedure within a muffle furnace, at temperatures ranging from 260°C to 300°C, for a period of 5 hours. This slow cooling process allowed the glass to gradually reach room temperature, effectively preventing the development of any internal stresses.

Table 1. Chemical composition (mol%) of the investigated glasses.

Sample name	Glass composition		
	PbO	B_2O_3	AlF_3
70Pb30B	70	30	0
60Pb30B10A	60	30	10
50Pb30B20A	50	30	20
60Pb20B20A	60	20	20
70Pb10B20A	70	10	20
70Pb20B10A	70	20	10
63Pb23B13A	63.4	23.3	13.3
55Pb27B17A	55	27.5	17.5
65Pb17B17A	65	17.5	17.5
65Pb27B7A	65	27.5	7.5

In carrying out the preparation procedure for a glass sample requiring differential thermal analysis, the sample was meticulously ground into a fine powder, using an agate pestle and mortar for this purpose. This powdered sample was then sifted through a sequence of standardized sieves. The portion that passed through a 270 mesh (53 μm) sieve was chosen for further analysis. The DTA analysis was conducted using a Derivatograf Q-1500D. High-purity alumina powder served as the reference substance. The following parameters were measured by subjecting the glass sample to a constant heating rate of 5°C/min, from room temperature to 1000°C in an air atmosphere: glass transition temperature (T_g), onset crystallization temperature (T_x), peak

crystallization temperature (T_c), and melting temperature (T_m). The determination of the glass transition temperature (T_g) was based on the initiation point of the first endothermic deviation observed in the DTA trace [17]. The process for identifying crystalline phases associated with exothermic peaks in differential thermal analysis (DTA) curves involved heat-treating glass powder in the air at the crystallization temperature for a duration of 5 hours. The emergence of crystalline phases post-heat treatment was ascertained via a DRON-3M X-ray diffractometer employing Co-K_α radiation to survey angles from 10 to 90 degrees (2Θ). The morphology of these crystalline phases within the glass-ceramic samples was then scrutinized using a field emission scanning electron microscope (MIRA3 TESCAN) set to a 10 kV operating voltage.

Fourier-Transform Infrared (FTIR) transmission spectra were collected with a Thermo Nicolet Avatar 370 FTIR Spectrometer in the 1400–400 cm^{-1} range at a 2 cm^{-1} resolution. The samples were prepared by blending 2 mg of glass powder with 200 mg of KBr, ground in an agate mortar, and then compressed into 13 mm diameter pellets. The recorded spectrum for each sample represents an average of 32 scans, standardized against a blank KBr pellet baseline [18].

Physical properties of the glass samples, such as the dilatometric softening point (T_d), the glass transition temperature (T_g), and the coefficient of thermal expansion (CTE), were determined using a dilatometer (model 1300 L, Italy) with a consistent heating rate of 3°C/min. The CTE was specifically evaluated over a temperature range from 20°C to 200°C. Additionally, the density of these glass samples was measured at ambient temperature utilizing the Archimedes principle with distilled water as the immersion medium.

3. Results and discussion

Figure 1 shows the powder X-ray diffraction (XRD) pattern of the prepared glass samples, which was performed in the range of 2Θ between 10° and 90° at room temperature. XRD analysis is a valuable tool for discerning the structural characteristics of materials, and the broad halo pattern observed in the XRD analysis of the glass samples is a clear indication of their amorphous nature. This feature arises from the short-range atomic order and the disordered atomic structure of amorphous materials, contrasting sharply with the well-defined diffraction peaks typically seen in crystalline materials. The absence of sharp peaks and the presence of a broad hump in the XRD pattern in the region of approximately 25° to 40° provide unambiguous evidence of the amorphous nature of the prepared glass samples.
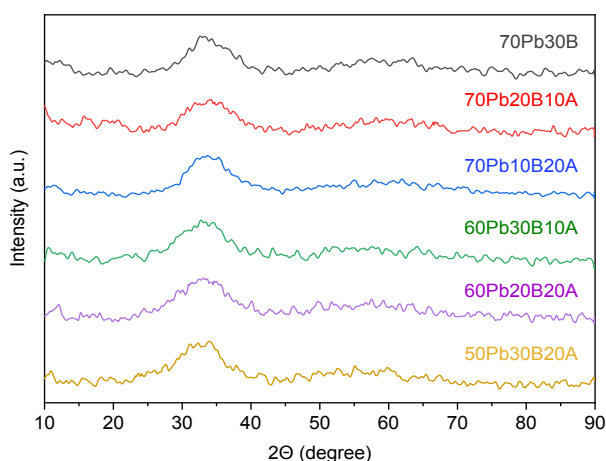

Fig. 1. XRD patterns of selected glasses.

The addition of AlF$_3$ significantly influences the local structure of lead borate glass, as evidenced by the analysis of their FTIR spectra, presented in Figure 2. FTIR spectroscopy yields crucial insights into the alterations in local structural units correlating with the glass composition. By analyzing the shape and position of infrared bands, one can infer potential modifications in the borate structural units of the examined glasses. The FTIR spectra reveal five major absorption bands (480, 710, 860, 1010, and 1240 cm^{-1}), whose intensities vary with the glass composition. These bands are broad and overlap due to the presence of different structural units, requiring the use of a Gaussian function for deconvolution. This deconvolution process separates the broad bands into distinct peaks, each representing a different structural unit. The deconvoluted peaks have two main characteristics: the center, which relates to the vibrations of specific structural groups, and the relative area, indicating the concentration of these groups [19]. Figure 3 displays the deconvoluted peaks for the investigated glass samples.
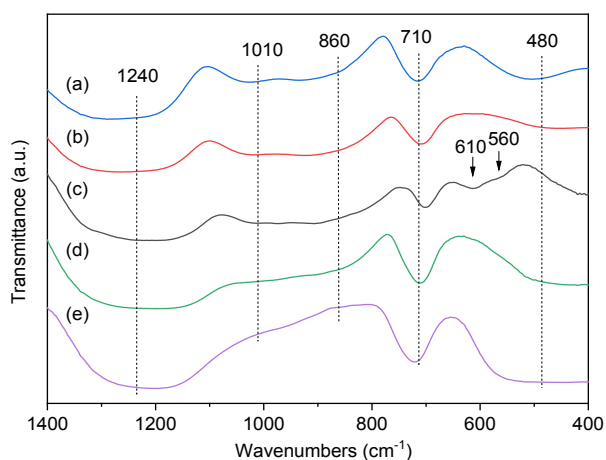

Fig. 2. FTIR plot of the (a) 50Pb30B20A, (b) 60Pb30B10A, (c) 70Pb30B, (d) 70Pb20B10A,
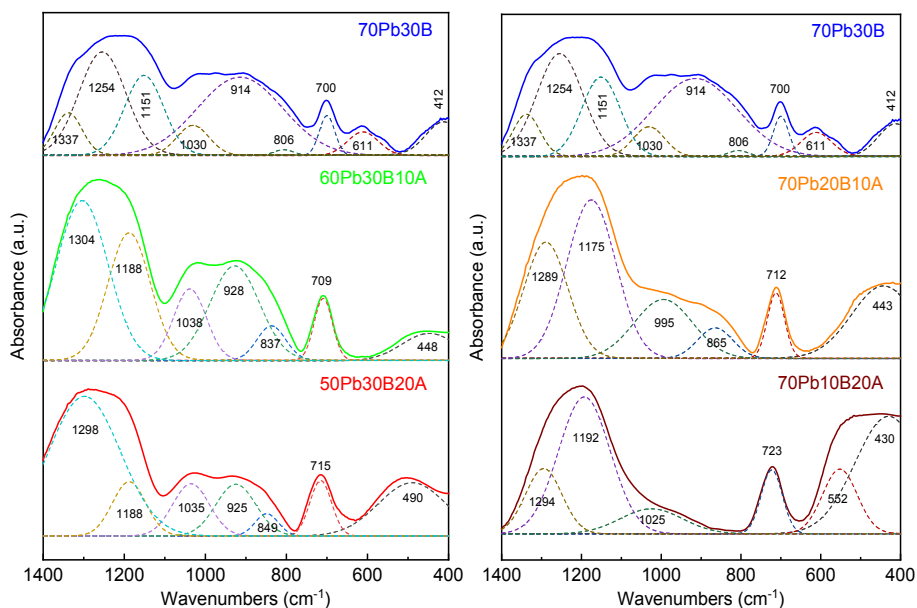*(e) 70Pb10B20A glasses.*

Fig. 3. Deconvoluted FTIR spectra of selected glasses.

The interpretation of FTIR spectra and identification of absorption bands involved consulting existing literature on lead borate and aluminoborate glasses [3, 20–22]. Borate-based glasses, primarily composed of different B_xO_y structural groups, are influenced by the type and concentration of the added modifiers, which determine the nature and concentration of these structural units within the glass structure [23]. A notable aspect is the role of PbO, which acts as a conditional glass former. This leads to the creation of specific structural units such as PbO_4 (quadrangular pyramid) and PbO_3 (triangular pyramid) [24]. In Fig. 2c, nine deconvoluted peaks are evident in the base glass at positions 412, 611, 700, 806, 914, 1030, 1151, 1254, and 1337 cm^{-1}. Many of these peaks were previously identified in the research conducted by Doweidar et al. [20], who investigated the structure of lead borate glasses doped with Al_2O_3. The spectral bands appearing in the 800–1100 cm^{-1} range are generally associated with borate structures that contain BO_4 groups. In contrast, the bands within the 1100–1400 cm^{-1} spectrum are linked to borate groups incorporating BO_3 units with non-bridging oxygen ions (NBOs) [3, 20]. The increase in the intensity and area of bands in the 1100–1400 cm^{-1} range with equimolar substitution of PbO or B_2O_3 by AlF_3 indicates an increase in the concentration of BO_3 units, while the decrease in band intensity in the 800–1100 cm^{-1} range suggests a reduction in the concentration of BO_4 units. Additionally, adding AlF_3 enhanced the absorption band at 700 cm^{-1}, attributed to the vibration of PbO_4 units and bending vibrations in BO_3 triangles, and suppressed the band at 611 cm^{-1}, which is related to the bending vibrations of B–O–Pb bonds within the glass network [3, 22]. A new band at 552 cm^{-1} in 70Pb10B20A glass, attributed to AlO_6 units [3], suggests a transformation of AlO_4 to AlO_6 units by converting BO_4 to BO_3 units. The study also noted a broad band at 430–490 cm^{-1}, linked to the symmetric bending vibration of the Pb–O bond in PbO_4 tetrahedra, and a band at 412 cm^{-1}, attributed to vibrations of Pb^{2+} ions [20–22].

Differential thermal analysis was employed to study the thermal properties of investigated glasses. The DTA results (Fig. 4) showed that, consistent with prior research [25, 26], the glass transition temperature (T_g) and other characteristic temperatures rise with increased heating rates. This trend is attributed to higher heating rates delivering more heat per unit of time, influencing the glass transition process. Essentially, as the heating rate increases, so does T_g due to a decrease in relaxation time, which becomes comparable to the isothermal holding time. This principle also affects the nucleation and crystallization of glass. At lower heating rates, more nucleation sites form, and crystallization starts at lower temperatures, whereas higher rates lead to faster crystallization and larger crystallites. These observations support existing literature [27] and highlight the crucial role of heating rate in determining the properties of glass during thermal processes.
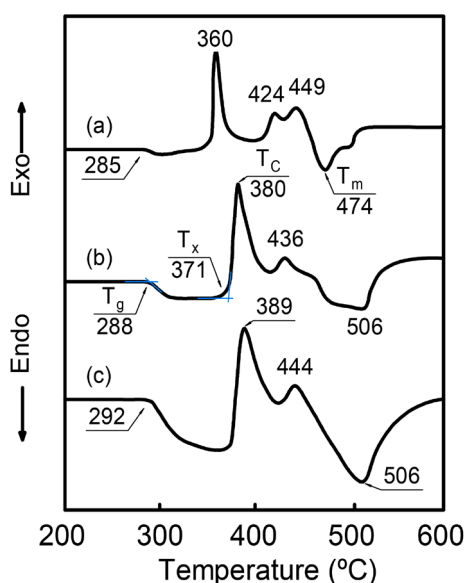

Fig. 4. DTA results of 70Pb30B sample at different heating rates: (a) 2.5 °C/min, (b) 5 °C/min and (c) 10 °C/min.

Fig. 5 presents DTA curves for various glasses at a constant heating rate of 5°C/min, providing insights into various characteristic temperatures, including melting and crystallization temperatures. These findings, including the specific temperature values, are compiled in Table 2. It was observed that all samples displayed an endothermic transition between 260 and 330°C, aligning with the T_g and confirming their glassy nature. Substituting PbO with AlF_3 in glass increases T_g due to the higher bond enthalpy of Al–F (664 kJ/mol) compared to Pb–O (378 kJ/mol) [28], while replacing B_2O_3 with AlF_3 decreases T_g, as the B–O bond (806 kJ/mol) is stronger than the Al–F bond. The study also found that substituting PbO with AlF_3 in the glass composition increased all characteristic temperatures, whereas replacing B_2O_3 with AlF_3 resulted in a lower T_g, T_x, and T_c but a higher T_m.
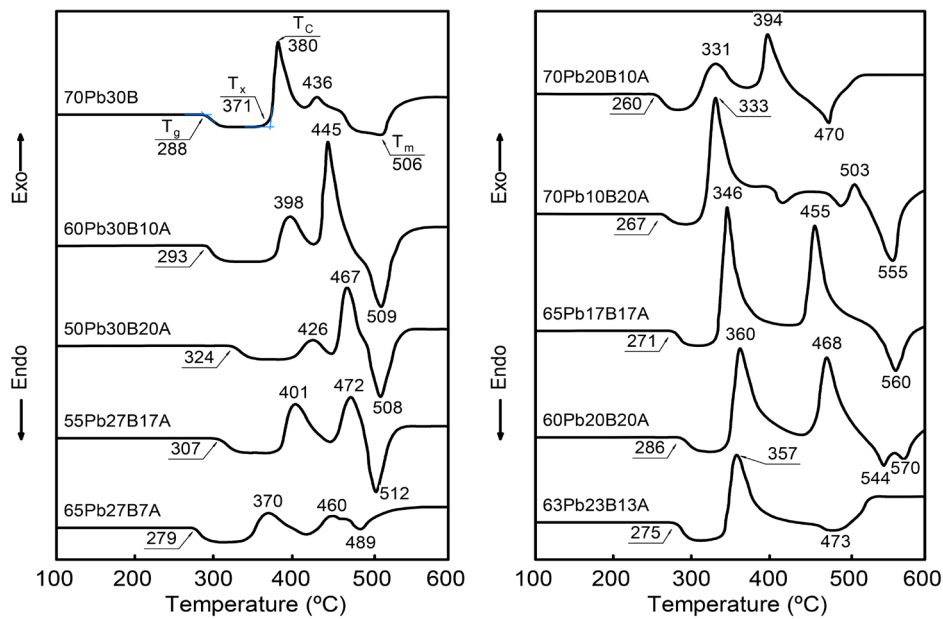

Fig. 5. DTA curves of investigated glasses using fine powders with a heating rate of 5 °C/min.

Table 2. Values of the characteristic temperatures (T_g, T_x, T_c, T_m), stability parameters (T_{gr}, ΔT, Hr), and density (ρ) of the investigated glasses.

Sample name	ρ, g/cm³	DTA				Stability parameters		
		T_g, °C	T_x, °C	T_c, °C	T_m, °C	T_{gr}	ΔT, °C	Hr
70Pb30B	6.87	288	371	380	506	0.57	83	0.73
60Pb30B10A	6.4	293	373	398	509	0.58	80	0.95
50Pb30B20A	5.98	324	401	426	508	0.64	77	1.24
60Pb20B20A	6.59	286	347	360	544	0.53	61	0.40
70Pb10B20A	7.17	267	312	333	555	0.48	45	0.30
70Pb20B10A	6.97	260	300	331	470	0.55	40	0.51
63Pb23B13A	6.59	275	341	357	473	0.58	66	0.71
55Pb27B17A	6.28	307	385	401	512	0.60	78	0.85
65Pb17B17A	6.76	271	332	346	560	0.48	61	0.35
65Pb27B7A	6.71	279	345	370	489	0.57	66	0.76

Most glass samples exhibited two distinct crystallization points, correlating to the formation of different crystalline phases influenced by compositional changes. To ascertain the phases formed during each exothermic peak in the DTA curves, the glass powders were heat-treated for 5 hours in air at their respective peak crystallization temperatures. Phase identification was conducted via powder diffraction file analysis. The peak crystallization temperatures varied

among compositions, with notable differences observed in the resulting crystalline phases, as demonstrated in the XRD patterns (Fig. 6). For instance, heat treatment at 380°C of the base glass (70Pb30B) led to the formation of $Pb_4B_2O_7$ (PDF 00-003-0576) and PbO (PDF 03-065-1471). The 63Pb23B13A glass, with 13 mol% AlF_3, predominantly formed Pb_2O_3 (PDF 00-023-0331) at 390°C. In the case of the 50Pb30B20A glass, the main crystallization product was PbB_2O_4 (PDF 00-020-0576). The addition of aluminum fluoride alters the main crystalline phase and crystal morphology, as shown in Fig. 7, where different glass compositions result in diverse crystal shapes: platelet and spherical for 70Pb30B, spherical for 63Pb23B13A, and flat prismatic for 50Pb30B20A. This comprehensive analysis underscores the intricate interplay between composition, thermal treatment, and the resulting structural and morphological changes in glass materials.
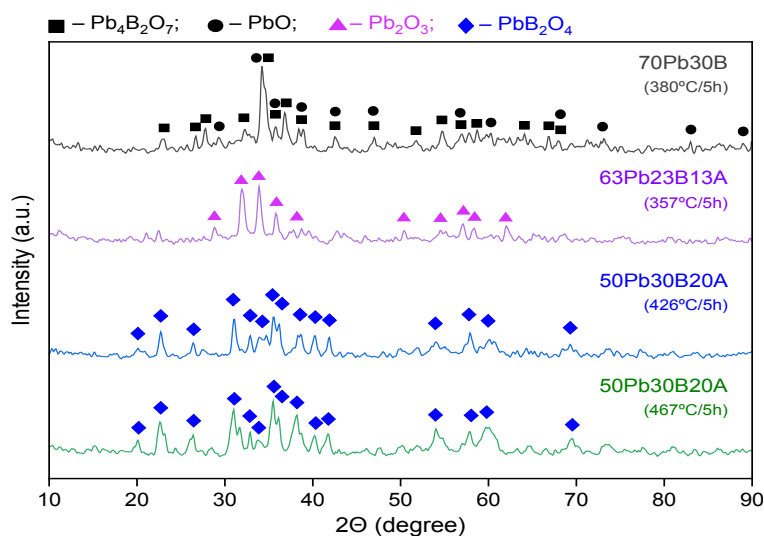

Fig. 6. XRD patterns of glass powders heat treated at the peak crystallization temperature for 5 hours.
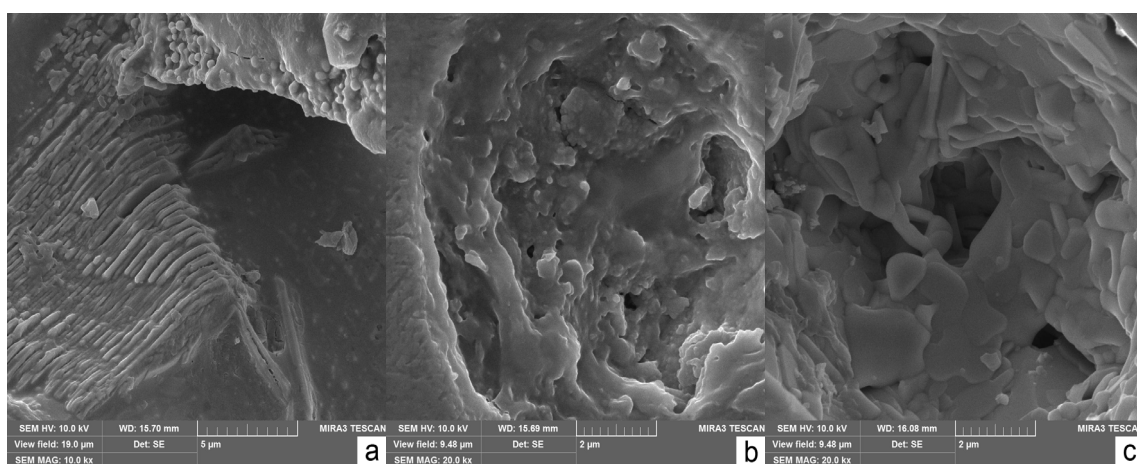

Fig. 7. SEM micrograph of the fractured surface of glass-ceramic samples derived from the 70Pb30B (a), 63Pb23B13A (b) and 50Pb30B20A (c) glasses after undergoing a 5-hour heat treatment.

Glass stability is a critical aspect of understanding the behavior of glass materials under heating. It measures the ability of glass to retain its amorphous structure and resist crystallization (devitrification) when heated. Assessing glass stability involves evaluating parameters that reflect the material's resistance to crystallization at different temperatures. The parameters help in

understanding the sintering window and the crystallization mechanism, which is vital for developing high-performance glass materials in various fields such as electronics, optics, and energy storage. The Dietzel parameter ($\Delta T = T_x - T_g$) and the Hruby parameter ($Hr = (T_c - T_g)/(T_m - T_c)$) are two primary examples [29, 30]. These parameters provide insights into the glass's thermal stability and its resistance to devitrification, which is crucial for maintaining its amorphous nature. A larger ΔT value, for instance, suggests higher thermal stability, indicating a broader sintering window, the temperature range within which glass can be processed without crystallizing [27]. Incorporating AlF_3 into lead borate glasses, as shown in Table 2, results in a reduction of the ΔT value. This suggests that AlF_3 serves as an efficient nucleation agent in these types of glasses. Hr values, indicative of glass formation ease, show that glasses with lower Hr values (<0.1) are more challenging to form and require rapid quenching, whereas those with higher Hr values (>0.4) indicate easier formation and stability at moderate cooling rates [31]. The substitution of PbO with AlF_3 in the base glass notably increases Hr values, enhancing the glass's stability, while the equimolar substitution of B_2O_3 with AlF_3 decreases them. The reduced glass transition temperature (T_{gr}) is another parameter, with values below 0.58–0.60 suggesting volume crystallization and values above 0.58–0.60 indicating surface crystallization [32]. A T_{gr} in the range of 0.58–0.60 implies no dominant crystallization mechanism. The replacement of PbO with AlF_3 in a glass composition significantly increases the reduced glass transition temperature from 0.57 to 0.64. This change in T_{gr} values suggests a notable shift in the crystallization behavior of the glass. A higher T_{gr} value, in this case exceeding the threshold of 0.60, typically indicates a transition from volume (homogeneous) crystallization to surface (heterogeneous) crystallization.

The dilatometric properties of glasses, including thermal expansion, glass transition temperature, and dilatometric softening temperature, are fundamental in understanding their behavior under various temperature conditions [33]. These properties are intrinsically linked to the glass's composition and structure, necessitating detailed studies to predict and control the thermal behavior of different types of glasses. The data from dilatometry (referenced in Fig. 8) illustrates how the equimolar substitution of PbO and B_2O_3 with AlF_3 in base glass composition results in significant changes in the dilatometric properties.
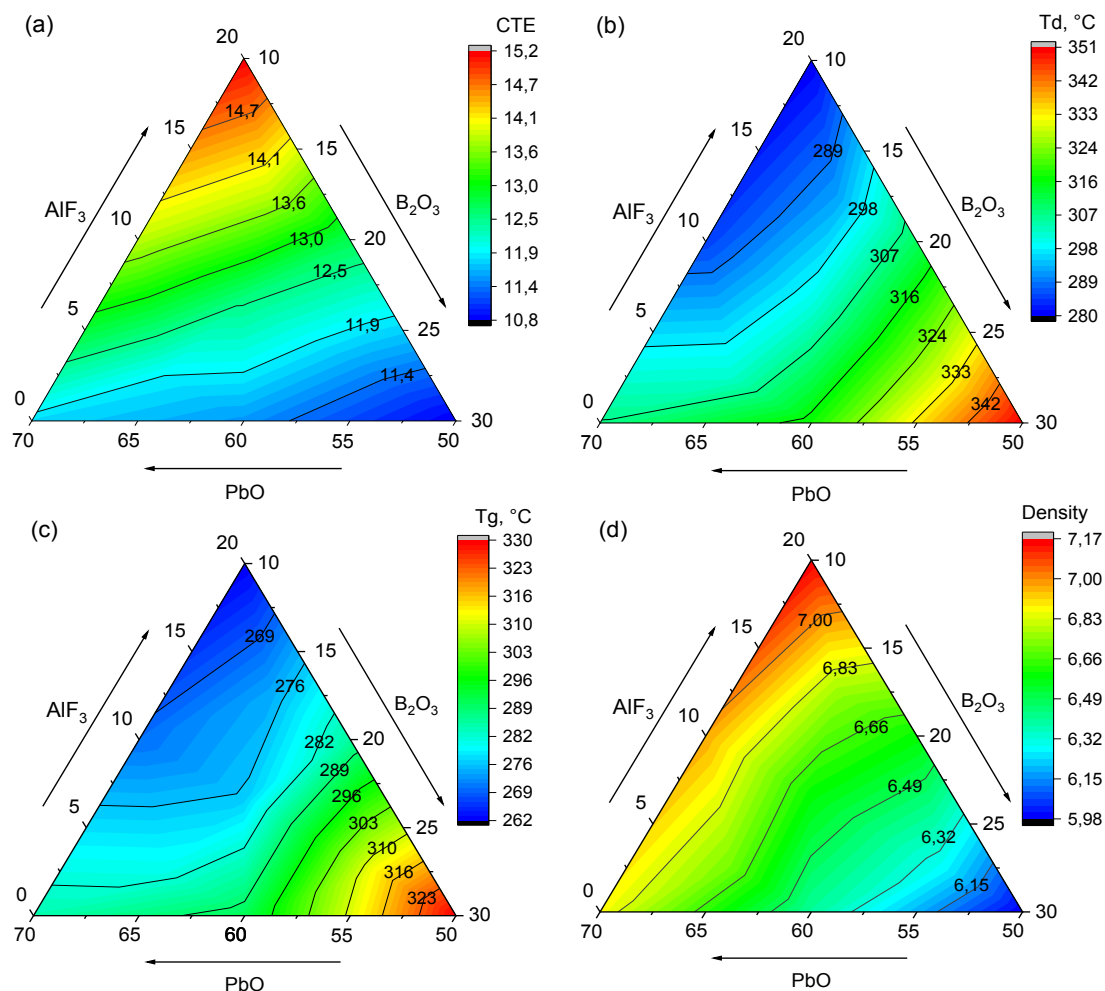
Fig. 8. Ternary plots of coefficient of thermal expansion (a), dilatometric softening point (b), glass transition temperature (c) and density (d) as a function of composition in the PbO–B$_2$O$_3$–AlF$_3$ glass system.

When PbO is replaced by AlF$_3$, there is an increase in both T$_g$ (from 285 to 330 ℃) and T$_d$ (from 307 to 351 ℃), accompanied by a decrease in the coefficient of thermal expansion (CTE) from 11.8 to 10.8 ppm/℃. This change is attributed to replacing weaker Pb−O bonds (378 kJ/mol) with stronger Al−F bonds (664 kJ/mol), enhancing the glass structure's rigidity and resistance to thermally induced contraction. Conversely, substituting B$_2$O$_3$ with AlF$_3$ leads to a decrease in T$_g$ (from 285 to 262 ℃) and T$_d$ (from 307 to 280 ℃), while the CTE increases from 11.8 to 15.2 ppm/℃. This trend is due to the substitution of stronger B−O bonds (806 kJ/mol) with weaker Al−F bonds (664 kJ/mol), leading to an increase in non-bridging bonds and network depolymerization, thereby reducing the glass structure's rigidity and increasing its thermal expansion. Additionally, Fig. 8d illustrates the variation in density as a function of glass composition. Density increases from 6.87 to 7.17 g/cm^3 when B$_2$O$_3$ is replaced by AlF$_3$ and decreases from 6.87 to 5.98 g/cm^3 with the substitution of PbO by AlF$_3$, reflecting the additive nature of density in relation to the densities of the substituted oxides: B$_2$O$_3$ (2.46 g/cm^3) < AlF$_3$ (2.88 g/cm^3) < PbO (9.53 g/cm^3). These findings underscore the complex relationship between glass composition, structural properties, and thermal behavior, offering valuable insights for developing glass materials with tailored properties for specific applications.

4. Conclusions

New oxyfluoride glass series with the formula $(70-x)\text{PbO}–(30-y)\text{B}_2\text{O}_3–(x+y)\text{AlF}_3$, where x and y range from 0 to 20 mol%, were produced using the conventional melt-quenching-annealing method. The thermal characteristics and crystallization behavior of the obtained glasses were examined using DTA, XRD, FTIR, SEM, and dilatometry. The findings showed that X-ray diffraction analysis affirmed the glasses' amorphous nature, highlighting their distinctive non-crystalline structure. Analysis of FTIR spectra revealed structural changes, particularly in the formation and increase of non-bridging bonds and the transformation of BO_4 to BO_3 units, which correlate with the increased addition of AlF_3.

Differential thermal analysis provided valuable insight into the characteristic temperatures and stability of the resulting glasses. The addition of AlF_3 influenced these temperatures, reducing them when replacing B_2O_3 and increasing them when replacing PbO. Crystalline phases were identified via XRD and SEM micrographs after heat-treating selected samples at the peak crystallization temperature.The density and thermal expansion values of lead borate glass changed with the addition of AlF_3, showing a decrease when AlF_3 replaced PbO and an increase when it replaced B_2O_3.

This work lays the groundwork for future research in optimizing the composition of oxyfluoride glasses for both scientific and practical applications.

Acknowledgements

References

[1] B. V. Padlyak, I. I. Kindrat, A. Drzewiecki, V. I. Goleus, Y. S. Hordieiev, J. Non Cryst. Solids **557**, 120631 (2021); https://doi.org/10.1016/j.jnoncrysol.2020.120631
[2] A. S. Abouhaswa, Y. S. Rammah, S. E. Ibrahim, R. El-Mallawany, Journal of Electronic Materials **48**, 5624 (2019); https://doi.org/10.1007/s11664-019-07391-4
[3] Yu. S. Hordieiev, A. V. Zaichuk, MRS Advances **8**(5), 201 (2023); https://doi.org/10.1557/s43580-023-00511-7
[4] C. Erdogan, M. Bengisu, S. A. Erenturk, Journal of nuclear materials **445**(1-3), 154 (2014); https://doi.org/10.1016/j.jnucmat.2013.10.025
[5] A. V. Nosenko, Y. S. Hordieiev, V. I. Goleus, Voprosy Khimii i Khimicheskoi Tekhnologii **1**, 87 (2018).
[6] G. ALMisned, D. Sen Baykal, G. Kilic, G. Susoy, H. M. H. Zakaly, A. Ene, H. O. Tekin, Applied Rheology. **32**, 178 (2022); https://doi.org/10.1515/arh-2022-0133
[7] M. Kurudirek, J. Alloys Compd. **727**, 1227 (2017); https://doi.org/10.1016/j.jallcom.2017.08.237
[8] V. Naresh, S. Buddhudu, Phys. Chem. Glasses Eur. J. Glass Sci. Technol. B. **56**, 255 (2015);. https://doi.org/10.13036/17533562.56.5.255
[9] J. Pisarska, W.A. Pisarki, J. Optoelectron Adv. Mater. **5**, 2667 (2005).
[10] B. V. Padlyak, I. I. Kindrat, Y. O. Kulyk, Y. S. Hordieiev, V. I. Goleus, R. Lisiecki, Mater. Sci. Eng. B Solid State Mater. Adv. Technol. **293**, 116460 (2023); https://doi.org/10.1016/j.mseb.2023.116460
[11] H. A. A. Sidek, S. Rosmawati, A. K. Yahya, Chalcogenide Letters **13**(4), 169 (2016).
[12] M. A. P. Silva, V. Briois, M. Poulain, Y. Messaddeq, S. J. Riberio, Journal of Optoelectronics and Advanced Materials, **4**, 799 (2002).
[13] Yu. S. Hordieiev, A. V. Zaichuk, Chalcogenide Letters **19**(12), 891 (2022); https://doi.org/10.15251/CL.2022.1912.891
[14] C. Maalegoundla, G. Sangeetha, K. C. Sekhar, D. Sreenivasu, M. Shareefuddin, J. Mater. Sci.: Mater. Electron. **34**, (2023); https://doi.org/10.1007/s10854-023-11534-z

[15] J. C. M'Peko, J. E. De Souza, S. S. Rojas, A. C. Hernandes, J. Appl. Phys. **103**, 044908 (2008); https://doi.org/10.1063/1.2885342

[16] Y. Wang, A. Osaka, Y. Miura, J. Non Cryst. Solids. **112**, 323 (1989); https://doi.org/10.1016/0022-3093(89)90546-2

[17] Yu. S. Hordieiev, E. V. Karasik, A. V. Zaichuk, Silicon **15**, 1085 (2023); https://doi.org/10.1007/s12633-022-01745-0

[18] Yu. S. Hordieiev, A. V. Zaichuk, J. Inorg. Organomet. Polym. Mater. **33**(2), 591 (2023); https://doi.org/10.1007/s10904-022-02526-3

[19] A. Abd El-Moneim, M. A. Azooz, H. A. Hashem, A. M. Fayad, R. L. Elwan, Sci. Rep. **13**, 12788 (2023); https://doi.org/10.1038/s41598-023-39489-5

[20] H. Doweidar, K. El-Egili, G. El-Damrawi, R. Ramadan, Phys. Chem. Glasses-Eur. J. Glass Sci. Technol. B **49**, 271 (2008).

[21] C. Gautam, A. K. Yadav, A. K. Singh, International Scholarly Research Notices **2012**, 428497 (2012); https://doi.org/10.5402/2012/428497

[22] S. G. Motke, S. P. Yawale, S. S. Yawale, Bulletin of Materials Science **25**, 75 (2002); https://doi.org/10.1007/bf02704599

[23] E. R. Shaaban, M. Shapaan, Y. B. Saddeek, J. Phys. Condens. Matter. **20**, 155108 (2008); https://doi.org/10.1088/0953-8984/20/15/155108

[24] B. V. Padlyak, I. I. Kindrat, Y. O. Kulyk, S. I. Mudry, A. Drzewiecki, Y. S. Hordieiev, V. I. Goleus, R. Lisiecki, Mater. Sci. Eng. B Solid State Mater. Adv. Technol. **278**, 115655 (2022); https://doi.org/10.1016/j.mseb.2022.115655

[25] Y. S. Hordieiev, A. V. Zaichuk, Journal of Ovonic Research **19**, 471 (2023); https://doi.org/10.15251/jor.2023.194.471

[26] S. Pawaria, M. Bala, H. Duhan, N. Deopa, S. Dahiya, A. Ohlan, R. Punia, A.S. Maan, J. Therm. Anal. Calorim. **147**, 13099 (2022); https://doi.org/10.1007/s10973-022-11531-0

[27] S. S. Danewalia, K. Singh, S. K. Arya, J. Non Cryst. Solids. **553**, 120471 (2021); https://doi.org/10.1016/j.jnoncrysol.2020.120471

[28] Y. R. Luo, Comprehensive Handbook of Chemical Bond Energies, CRC Press, (2007); https://doi.org/10.1201/9781420007282

[29] A. Dietzel, Glasstech Ber. **22**, 41 (1968).

[30] A. Hrubý, Czechoslov. J. Phys. **22**, 1187 (1972); https://doi.org/10.1007/bf01690134

[31] I. G. Geidam, R. El-Mallawany, N. Nazrin, M. N. Baba, Journal of Theoretical and Applied Physics **16**(2), 1 (2022); https://doi.org/10.30495/jtap.162220

[32] V. Dua, S. K. Arya, K. Singh, J. Mater. Sci. **58**, 8678–8699 (2023); https://doi.org/10.1007/s10853-023-08567-4

[33] E. V. Karasik, Yu. S. Hordieiev, Voprosy Khimii i Khimicheskoi Tekhnologii **6**, 69 (2020); https://doi.org/10.32434/0321-4095-2020-133-6-69-74